Annals of Nuclear Energy 109 (2017) 529–537

Contents lists available at ScienceDirect

Annals of Nuclear Energy

journal homepage: www.elsevier.com/locate/anucene

A CFD-based simulation of fluid flow and heat transfer in the Intermediate Heat Exchanger of sodium-cooled fast reactor

Xiaolong Zhang *, Peichi Tseng, Muhammad Saeed, Jiyang Yu

Department of Engineering Physics, Tsinghua University, Beijing 100084, China

ARTICLE INFO

Article history:
Received 2 December 2016
Received in revised form 27 May 2017
Accepted 30 May 2017
Available online 9 June 2017

Keywords:
CFD
Sodium-cooled fast reactor
Porous media approach
Intermediate Heat Exchanger

ABSTRACT

A three-dimensional computational fluid dynamics (CFD)-based simulation for the Intermediate Heat Exchanger (IHX) of a pool-type sodium-cooled fast neutron reactor has been performed in this paper, which investigates the flow-field and temperature distributions of liquid sodium on both primary and secondary sides at full power conditions. Typically, some simplifications are applied to reduce the difficulty of computation and render the problem more tractable. A proposed method is that treat a number of tubes as porous media that replicates the pressure loss and heat transfer characteristics of the detailed model. The heat exchanger model of the ANSYS FLUENT code is used to analyze the heat transfer phenomena inside of the IHX and the resistance coefficients of porous media have been predicted by empirical relationships which vary with height and flow directions. Two separate models, with different size of inlet and outlet area for shell-side sodium, have been developed in this paper. By comparing the results from the different simulations, the model with larger inlet area for primary and non-uniform inlet velocity distribution of secondary sodium satisfies the design requirements with respect to the permissible upper limit of temperature difference and local radial velocity.

1. Introduction

The sole coolant in a pool-type sodium-cooled fast reactor is liquid metallic sodium, which has a wide range of temperature variation below the boiling point and it would remain liquid phase during normal operating conditions. The reactor is composed of two liquid sodium circuits and one steam circuit, which are reactor loop, intermediate loop, and power-generation loop, respectively (Gajapathy et al., 2008). The reactor and intermediate loop are connected by the Intermediate Hear Exchanger, which is a shell and tube heat exchanger that consists of a shell with a bundle of tubes inside it. The hot primary sodium carries heat from hot pool flow into the inlet grid of the IHX with a specified velocity distribution and rate, pass over the tube bundles (through the shell, so called the shell-side) and transfer the heat to the secondary sodium that flow though the tube bundles (the tube-side). The inlet and outlet window for primary sodium are designed at top and the bottom of the IHX respectively, as shown on Fig. 1.

The main purpose of this study is to investigate the flow-field and temperature distributions of liquid sodium inside the IHX, and to propose optimized designs using the computational fluid dynamics method. The analysis concentrates on the inequality of temperature distribution that brings about a great temperature gradient between inner and outer tube bundles. The hottest tube tries to expend more than the rest of the tube bundle, which reduces the stability of welding structure. Driven by gravity, if hot sodium in some channels that fully transfers heat to the secondary side, its density would change quickly. Hence, the flow rate will become larger automatically. While the heat exchange is not sufficient, the flow rate will not be enhanced, which results to a relatively lower flow rate and velocity. The fluid temperature change per unit length could be larger, therefore, under the same heat exchange condition, which will strengthen the natural circulation and increase the flow rate. It is a favorable feedback mechanism that contributes to reduce the average fluid temperature difference between different flow channels. But this mechanism cannot completely solve the problem of uneven temperature distribution. A large local fluid flow rate could cause flow-induced vibration, decrease the local heat transfer capacity. Thus, the maximum radial temperature difference of tube bundle is determined to be 20 K and the maximum radial velocity of primary sodium to be 0.73 m/s.

The design of Intermediate Heat Exchange is extremely complicated, with thousands of arranged heat transfer tube and locating rods. It is difficult to simulate each heat tube and the entire region

* Corresponding author.
E-mail address: xlzhang16@mails.tsinghua.edu.cn (X. Zhang).

http://dx.doi.org/10.1016/j.anucene.2017.05.063
0306-4549/

Nomenclature

CFD	Computational Fluid Dynamics
SFR	Sodium-cooled fast reactor
IHX	Intermediate Heat Exchanger
$\boldsymbol{C}$	Inertial resistance factors
De	Hydraulic diameter
d	Outer diameter of heat exchange tube
d_{in}	Inner diameter of heat exchange tube
f	the resistance coefficient
$\boldsymbol{f}$	Body force
K	Resistance coefficient in cross flow
L	Length along tube
Δn_i	Thickness of porous medium
p	Pressure
Re	Reynolds number
R_{in}	Inner radius of model
R_{out}	Outer radius of model
$\boldsymbol{S}$	Source term in the momentum equation
S_1	Circumferential distance
S_2	Radial distance
S_2'	Horizontal distance
T	Temperature
t	Time
U	Inlet velocity of shell-side sodium
$\boldsymbol{v}$	Velocity vector
V	Average flow rate
Z	Half number of tube bundles
α	Permeability of porous medium
ε	Surface roughness
ρ	Density
μ	Dynamic viscosity
τ	Stress tensor

Subscripts

pri	Primary side
sec	Secondary side
i	x, y, z coordinate directions

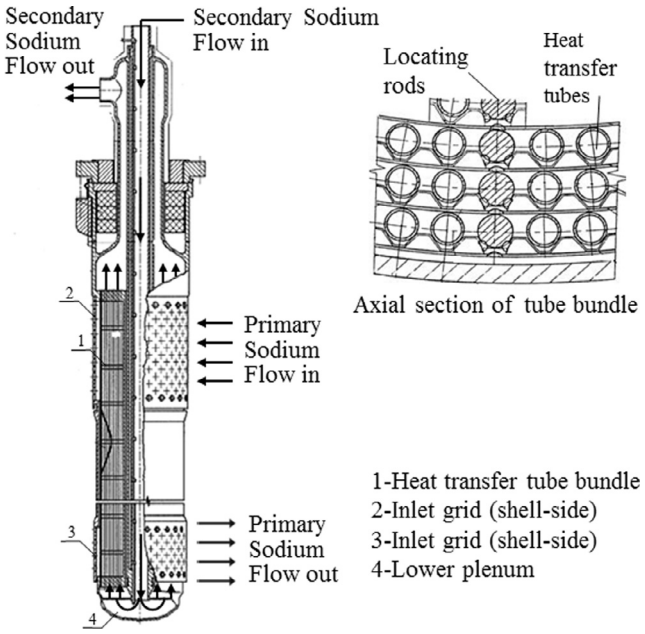

Fig. 1. Schematic view of the IHX.

in a detailed model. In the analysis of flow distribution characteristics, porous media approach is used to generate flow resistance and achieved heat exchange. In order to meet the design requirements, two geometry models with different inlet area of shell-side sodium have been developed in this work. In each model, the inlet velocity of the tube-side sodium is set to be uniform and non-uniform, simulated separately.

ANSYS FLUENT code provides the heat exchanger model, a solution to problems that consists of heat exchange happening in a lager tube bundle and unable to build a detailed model, which is suitable for this case (ANSYS Inc., 2013). The model that uses the lumped parameter method can greatly reduce the number of grids and easy to calculate. In fact, the role of the heat exchanger is to generate the pressure drop for primary side fluid and transfer the heat to the secondary side. In the ANSYS FLUENT, the secondary fluid is called the auxiliary fluid. The heat exchanger model is usually combined with a porous media method to calculate the overall pressure drop by inputting the resistance factors in the porous media to calculate the resistance.

Porous media approach is often performed in the simulation of single-phase or multi-phase fluid problems, including fluid through the filter paper, orifice plate, flow distributor and tube bundle (Tochio and Fujimoto, 2016; Boyd and Hardesty, 2003). Khair et al. (2008) accomplished the prediction of temperature distribution and coolant flow-field in the endshield of advanced CANDU designed by Atomic Energy of Canada Limited, which simplified the lattice tubes in the endshield as porous medium. Pilehvar et al. (2013) investigated the flow behavior in the core of a Pebble Bed Modular Reactor (PBMR), using porous media approach. Dehbi and Badreddine (2013) considered a comparison between detailed model and porous media simplification that replicated the heat transfer characteristics in a steam generator. In addition, Zarifi et al. (2013) accomplished a study that calculated the flow behavior of coolant as nanofluid in the VVER-1000 reactor core, using the porous media simplification. Furthermore, Suyambazhahan et al. (2014) performed an equivalent anisotropic porous medium approach to analyze the effects of flow distributor on the temperature distribution inside the IHX of a liquid metal-cooled fast breeder reactor (LMFBR). Although the porous media model lacks part of the detailed structure, it has the advantages of making the problem computationally tractable. In the early stage of an engineering project, this simplification can be useful to effectively compare various designs and raise improvements (Haibo et al., 2006; Wang et al., 2016).

2. Geometry description

In this work, only the heat transfer part of the Intermediate Heat Exchanger is modeled and simulated. The geometric model of this part is a hollow cylinder, as shown on Fig. 2. The primary-side sodium flow from the circumferential surface of the upper part of the model and flows out from the lower circumferential surface of the model; the secondary side of the sodium flows in from the annular surface at the bottom of the hollow cylinder and flows out from the annular surface at the top of the hollow cylinder. Two separate models, with different size of the inlet and outlet area for shell-side sodium, are developed in the paper.

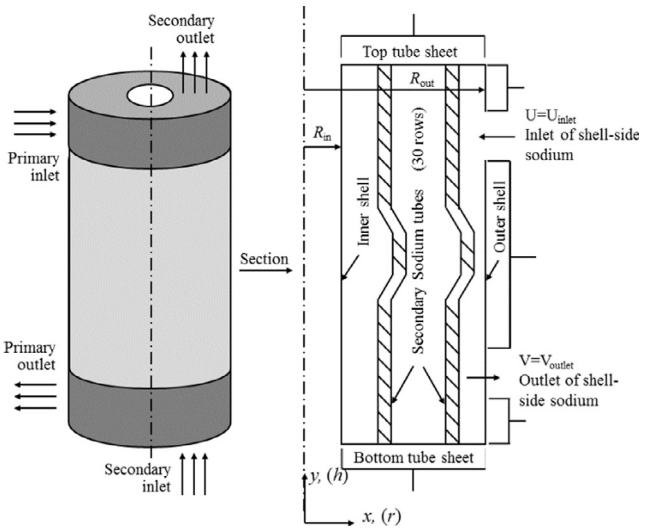

Fig. 2. Section of the Intermediate Heat Exchanger.

The model with a standard size of the inlet and outlet area for shell-side sodium is called the model 1. Another model enlarges the size of the inlet and outlet area to twice of the standard area, called model 2. Structured meshes are applied in the simulations. Each geometry has two different mesh, standard mesh and fine mesh, to ensure the solutions are independent of the grid. The average grid quantity of fine mesh of each model is above 3 million and each standard mesh has 2 million girds approximately.

3. Method of simulation

It is difficult to directly model each and every tube in the IHX, with the capability of the current computer. The effect of tube bundle is to offer pressure loss for both side flows and heat the tube-side sodium. Porous media model can achieve these functions. Therefore, porous media treatment has been adopted in the simulation to reduce the computational difficulty (Fig. 3). Porous media can provide fluid resistance and the Heat Exchanger Model in FLUENT code has been employed to deal with the heat transfer phenomenon. It should be highlighted that the accuracy of the simulation is not greatly degraded by the porous media approach. Pressure drop coefficients are evaluated by experimental correlations, which is a function of Reynolds number and geometry of fluid region in shell-side and tube-side.

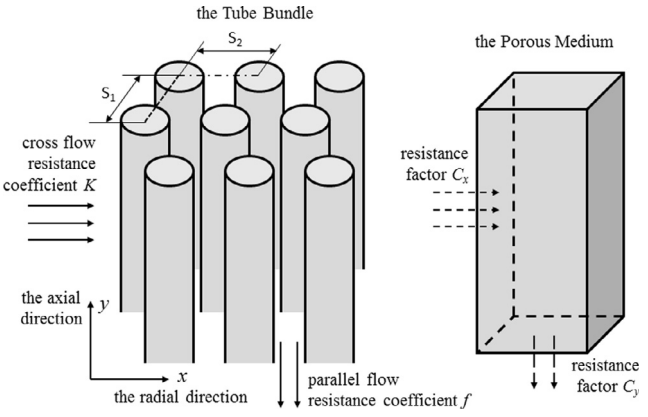

Fig. 3. The Tube Bundles and the Porous Medium.

3.1. Governing equations

Liquid sodium flowing inside the Intermediate Heat Exchanger is governed by the conservation equations of mass, momentum and energy in the porous media same as sodium flows thought an open space. These equations are presented below.

Continuity equation for three-dimensional flow is modified from the general form:

The continuity equation is:

$$\frac{\partial \rho}{\partial t} + \nabla \cdot (\rho \boldsymbol{v}) = 0 \tag{1}$$

The momentum equation for porous media is described by:

$$\frac{\partial}{\partial t}(\rho \boldsymbol{v}) + \nabla \cdot (\rho \boldsymbol{v}\boldsymbol{v}) = -\nabla p + \rho \boldsymbol{f} + \nabla \cdot \boldsymbol{\tau} + \boldsymbol{S} \tag{2}$$

where $\boldsymbol{v}$ is the superficial velocity in porous media, and $\boldsymbol{S}$ contains the additional momentum source terms of porous media, which consists of viscous loss (first term on the right-hand side of equation) and inertial loss (second term on the right-hand side of equation).

Considering a homogeneous porous media, source can be written as:

$$S_i = -\left(\frac{\mu}{\alpha} v_i + C_i \frac{1}{2} \rho |v| v_i\right) \tag{3}$$

When at low velocity, usually the Reynolds number less than a unity, pressure drop created by the source term is mainly viscous loss, which is proportional to the velocity of flow. In the case of Intermediate Heat Exchanger, it is not a laminar flow, therefore the first term can be ignored. Pressure drop focused on the second term, the inertial loss that takes into the convective acceleration and diffusion of flow. The inertial resistance factor, C_i for each direction is calculated by empirical correlations and set into the FLUENT code, then the code will be able to simulate the flow behavior in porous media.

3.2. Heat Exchanger Model in FLUENT (the Dual Cell model)

To analyze heat transfer process and temperature distribution of both shell and tube side sodium, the Dual Cell Model of FLUENT code has been used in the simulation. This model allows a non-uniform fluid that passes thought an arbitrary shaped heat exchanger core (ANSYS Inc., 2013). The dual cell refers to the two completely overlapping porous fluid simulation cell zones of the heat exchanger in the same physical space, respectively, the primary side area and the secondary side fluid area. Two zones are solved simultaneously and coupled through heat transfer.

The data that defines how the targeted heat rejection values relate to the fluid flow rates has been entered the code. As shown in Table 1.

3.3. The Resistance coefficient

At high flow velocities, the inertial resistance factor, C_i in Eq. (3) provides a correlation for inertial losses in the porous medium. This constant can be viewed as a loss coefficient per unit length along the flow direction, thereby allowing the pressure drop to be specified as a function of dynamic head. The simplified form of the porous media equation written in the term of the pressure drop in direction i is (Kaviany, 1995):

$$\Delta p_i \approx C_i \Delta n_i \frac{1}{2} \rho v_i |v| \tag{4}$$

where Δn_i is the thickness of the porous medium.

Table 1
The heat transfer data.

		Percent to the targeted tube-side fluid flow rate		
		0.9	1.0	1.1
		Percent to the targeted heat transfer		
Percent to the targeted shell-side fluid flow rate	0.9	0.92	0.94	0.96
	1.0	0.98	1.0	1.02
	1.1	1.03	1.05	1.08

For shell-side sodium, the resistance coefficients are calculated differently for cross flow (in the radial direction, the turbulent cross flow over the bundle) and parallel flow (in the axial direction, the flow is parallel to the tube axis).

The flow resistance coefficient K for turbulent passing over a bundle of smooth-wall staggered tubes is evaluated from empirical equations given by Idelchik (1966), as a function of bundle geometry and Reynolds number:

$$\Delta p = \frac{K\rho U^2}{2} \tag{5}$$

where,

$$K = \mathrm{A} * Re^{-0.27}(Z+1) \tag{6}$$

$$\mathrm{A} = 3.2 + \left(4.6 - 2.7\left(\frac{S_1 - d}{S_2' - d}\right)\right)\left(2.0 - \frac{S_1}{d}\right) \tag{7}$$

and

$$S_2' = \left(0.25S_1^2 + S_2^2\right)^{0.5}. \tag{8}$$

where U is the inlet velocity of shell-side sodium. Z is half number of tube bundles. While S_1, S_2 and S_2' are the distances between tubes in circumferential, radial and horizontal direction, respectively.

Therefore, the inertial resistance factor, $C_{x,\mathrm{pri}}$, is:

$$C_{x,\mathrm{pri}} = \frac{K}{R_{\mathrm{out}} - R_{\mathrm{in}}} \tag{9}$$

where R_{out} is the outer radius of the model and R_{in} is the inner radius. $C_{x,\mathrm{pri}}$ allows the pressure drop per unit length along the x direction generated by fluid flowing over the bundle to be the same as that of the fluid flowing though porous medium. And $C_{z,\mathrm{pri}}$ is equal to $C_{x,\mathrm{pri}}$.

For parallel flow of shell-side sodium, the pressure drop depends on the physical geometry of the pipe and the flow pattern. The resistance coefficient f is a friction loss factor of turbulent flowing through smooth pipes (Idelchik, 1966). It is calculated as:

$$\Delta P = \frac{fL\rho V^2}{2D_e} \tag{10}$$

where V is average flow rate. The friction factor f is given by the Altshul equation (Genić et al., 2011). The friction factor is found to be a function of the Reynolds number and the relative roughness, which can be expressed as:

$$f_{\mathrm{pri}} = 0.11\left(\frac{\varepsilon}{d} + \frac{68}{Re}\right)^{0.25} \tag{11}$$

Compare Eq. (10) with Eq. (4), the inertial resistance factor in the axial direction is:

$$C_{y,\mathrm{pri}} = \frac{f_{\mathrm{pri}}}{D_e} \tag{12}$$

For tube-side fluid, the friction factor f is calculated by Eq. (11), where d is the inner diameter of tube:

$$f_{\mathrm{sec}} = 0.11\left(\frac{\varepsilon}{d_{\mathrm{in}}} + \frac{68}{Re}\right)^{0.25} \tag{13}$$

The inertial resistance factor in the axial direction for tube-side sodium is expressed as:

$$C_{y,\mathrm{sec}} = \frac{f_{\mathrm{sec}}}{d_{\mathrm{in}}} \tag{14}$$

The secondary-side sodium only flow along the tubes, therefore the resistance factors in x and z direction are set to 1000 times of $C_{y,\mathrm{sec}}$, which will limit the movement of the fluid only along the axis.

The state data of the liquid sodium entered into FLUENT is listed in Table 2. In the above calculations, the density and the viscosity of sodium are taken at the average temperature, which are obtained by linear interpolation from Table 2.

3.4. Boundary conditions

The flow resistance coefficients of different directions can be obtained for both sides fluid by using Eq. (5) to Eq. (14). On Fig. 4, heat exchanger tube is divided into five sections, two inclined sections and three vertical sections. In the inclined sections, the conical coordinate system is chosen to set the inertial resistance factors. In conical system, there are three coordinate directions that are orthogonal to each other. Direction-1 is the tangential direction of the cone, Direction-2 is the normal to the cone surface and Direction-3 is the circumferential direction, as shown on Fig. 5. When the fluid flows along the Direction-1, it is considered as parallel flow. Hence, the inertial resistance factor is set to the same value as C_y. In Direction-2 and Direction-3, the flow is considered as cross flow. Therefore, the inertial resistance factors are equal to that in vertical sections.

The local resistance coefficient of the bending part of the pipe is K = 0.2 (Idelchik, 1966) and it has been added to the direction of the main flow. Table 3 shows the inertial resistance factors input the simulations.

The convergence criterion has been set to 1.0e−4 for the momentum, pressure and energy. The final residual of these parameters do not exceed the convergence criterion.

The realizable k − ε model is used to calculate the turbulence in the FLUENT.

Table 2
The state data of the sodium (Liu et al., 2013).

Temperature (°C)	Density (kg/m^3)	Viscosity (mPa·s)	Specific heat (kJ/kg·K)
300	880	0.340	0.363
400	856	0.278	0.355
500	823	0.239	0.351
600	818	0.212	0.349

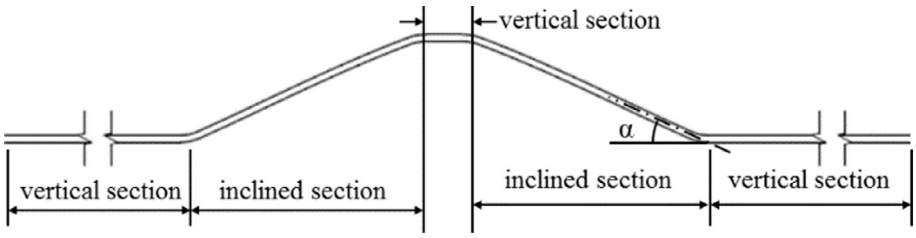

Fig. 4. Schematic diagram of heat transfer tubes.

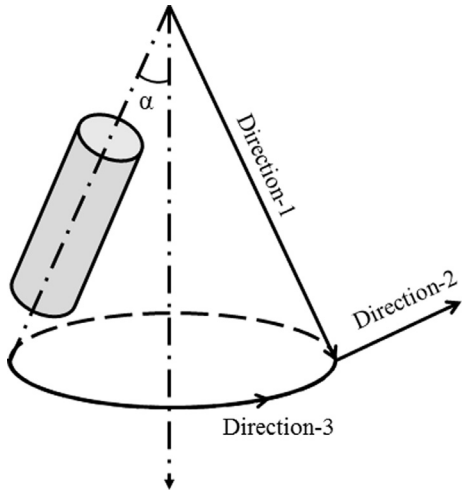

Fig. 5. The Conical Coordinate System.

Table 3
The inertial resistance factors of flow.

C_i (m^{-1})	Shell-side	Tube-side
y direction and Direction-1	14.31	18.00
x direction and Direction-2	2.16	1000 times of y direction
z direction and Direction-3	2.16	

3.5. Non-uniform inlet velocity of tube-side sodium

Based on the flow distribution results of lower plenum, the inlet area of tube-side sodium is divided into three areas with different velocity according to the radius: $R_1 = 600$mm, $R_2 = 900$mm (as shown on Fig. 6). The area 1 with a radius between R_{in} and R_1 is the innermost area, where the flow rate is set to $\bar{v}_1 = 0.55$m/s. The middle area with a relatively lower velocity of $\bar{v}_2 = 0.49$m/s, is between R_1 and R_2. And the flow rare on the outermost area is greater than the others with velocity of $\bar{v}_2 = 0.63$m/s.

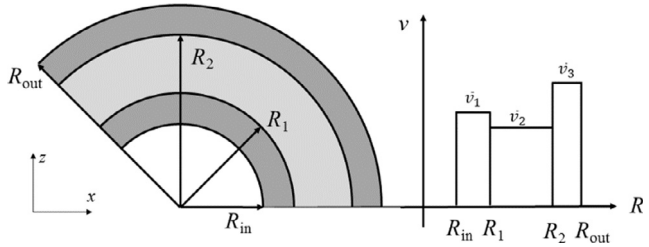

Fig. 6. Non-uniform inlet of tube-side sodium.

4. Results

As temperature of the solid skeletons of porous media cannot be predicted in this work therefore, the results take an approximation that predict the temperature of tube wall to be the average temperature of primary and secondary sodium, which is considered to be reasonable, because the wall is relatively thin, as shown in Fig. 7. The three vertical measuring lines are chosen to demonstrate the tube wall temperature, which are located at a radius of 419.5 mm, 727.5 mm and 1057.5 mm respectively, as shown in Fig. 8.

4.1. Uniform velocity inlet of tube-side sodium

The Table 4 shows the simulation results of some main parameters of the Intermediate Heat Exchanger, such as heat transfer power, the outlet sodium temperature in both insides and the targeted values, with the uniform tube-side sodium flow rate on the inlet.

The shell-side sodium temperature distribution on x – y plane is shown in Fig. 9. Hot sodium enters the IHX from the upper inlet grid, loses heat and temperature is decreasing. At same height, the temperature of shell-side near the inner tube bundles is lower than that of other tubes because heat has been transferred to the tube-side when flowing over tube bundles. As the fluid flow downward, the temperature drop gradually.

For the tube-side, the temperature of outer tubes rises faster than that of inner tubes at the same height, due to the higher temperature of shell-side sodium and more efficient heat exchange. After flowing through the inclined part of tube bundles in the middle, the temperature distribution is more uniform, the temperature difference between inner and outer tubes falling. Before tube-side sodium flow out the IHX, tubes at outer side contact with a hot

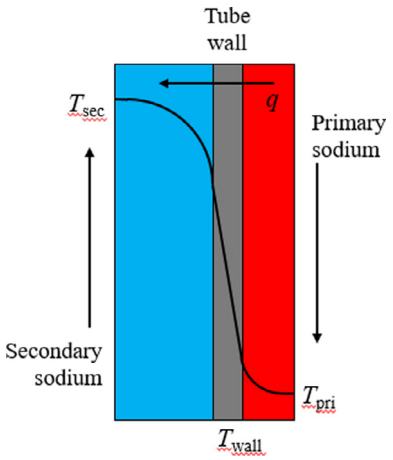

Fig. 7. The wall temperature of heat exchanger tubes.

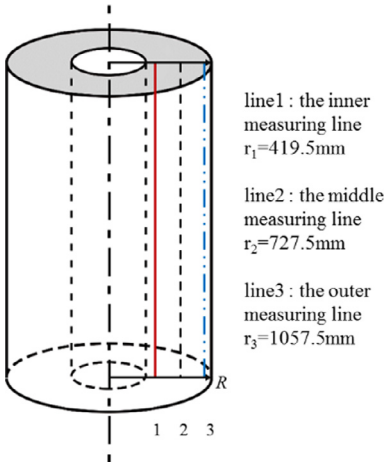

Fig. 8. Location of the three measuring lines.

sodium of shell-side directly, thus the temperature is higher than the inner row as shown on Fig. 9 and Fig. 10.

Fig. 11 and Fig. 12 show that the wall temperature of heat transfer tube on different rows of tube bundles (inner, middle and outer) corresponding to the axial height. The measuring temperature of the inner row and the middle row is quite close while the outer row always tends to be higher in both models and a departure between outer and inner curve is noted. In the range0 $\leqslant$ relative axial position $\leqslant$ 0.16, outer curve of model 1 rising more rapidly begins to depart from other two curves, causing a significant temperature difference. The slope of the outer curve is reducing gradually and approaching to the other curves.

There is a slight fall in the maximum temperature difference, after the secondary sodium enters the heat exchange tubes, bottoming out in both models, as shown on Fig. 13. The situation begins to deteriorate and the curve of model 1 rises dramatically from around 2 K to a peak of just under 40 K near the axial position of 1 m, which is twice as much as the design requirement of 20 K. Although the temperature difference of model 2 increases slower than model 1, it has a substantial growth as well reaching the highest point of 30 K near the relative axial position of 0.25, which is still far greater than the permissible upper limit of 20 K. Subsequently, the two curves decline gradually from the peak to below 10 K.

4.2. Non-uniform velocity inlet of tube-side sodium

The Table 5 shows the simulation results of some main parameters of the Intermediate Heat Exchanger, while the velocity inlet of tube-side sodium is set non-uniform, such as heat transfer power, the outlet temperature of both insides of sodium and the

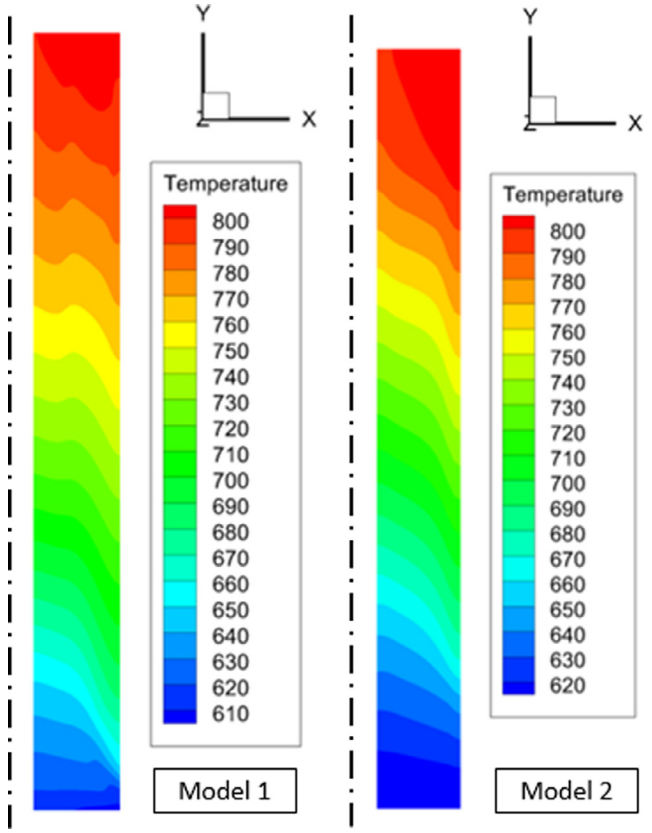

Fig. 9. Temperature distribution of shell-side sodium of model 1 and 2, uniform velocity.

assumed results, with the non-uniform tube-side sodium flow rate on the inlet.

The shell-side sodium temperature distribution on x – y plane is displayed in Fig. 14. Compared with the uniform condition, these two results show noticeable differences. In both models, the heat transfers in inner and outer regions have been enhanced by the increase of the flow rate of secondary sodium in the outer and inner tubes. Therefore, the shell-side sodium temperature is seen to be lower in these two regions than that in the middle and shell-side temperature distribution is more uniform in model 2, which is a favorable result. For the same reason, tube-sides sodium appears that the inner and outer rows are at higher temperatures (as shown on Fig. 15).

Fig. 16 and Fig. 17 show that the temperature of three measuring lines rise gradually in both models and the departures among the three curves is reduced significantly as compared with uniform

Table 4
Simulation results of main parameters of intermediate heat exchanger, uniform velocity.

	Model	Simulation results	Targeted values	Error (%)
Heat transfer (MW)	1	362.6	350	3.6
	2	357.5		2.13
Outlet Temperature of shell-side sodium (K)	1	628.71	625	0.57
	2	629.4		0.68
Outlet Temperature of tube-side sodium (K)	1	781.6	770	1.5
	2	774.3		0.56

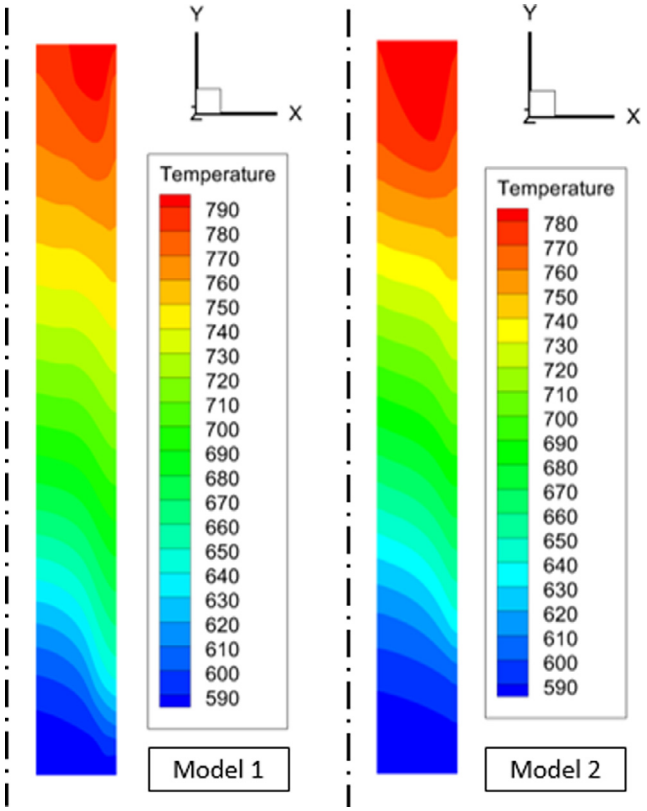

Fig. 10. Temperature distribution of tube-side sodium of model 1 and 2, uniform velocity.

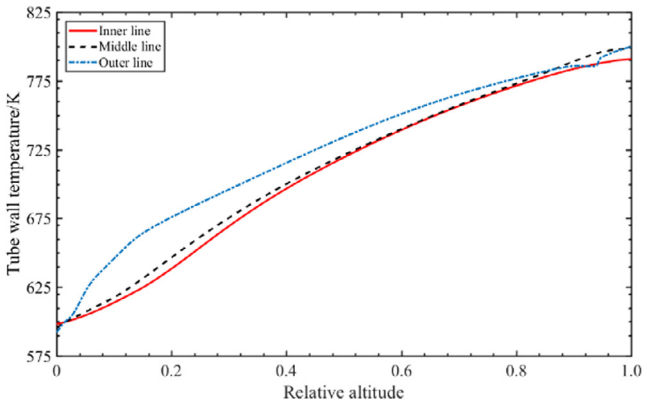

Fig. 11. The wall temperature vs. axial position, uniform velocity, model 1.

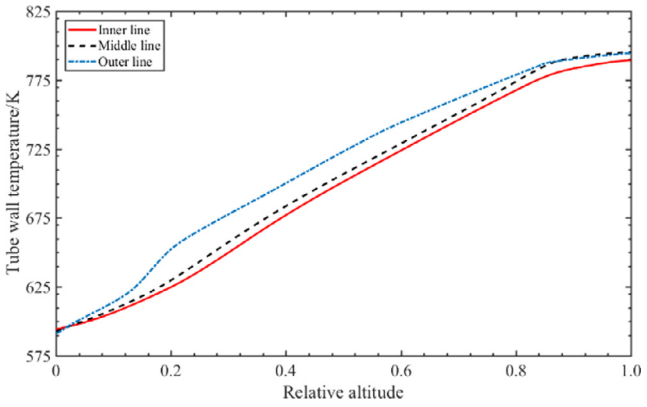

Fig. 12. The wall temperature vs. axial position, uniform velocity, model 2.

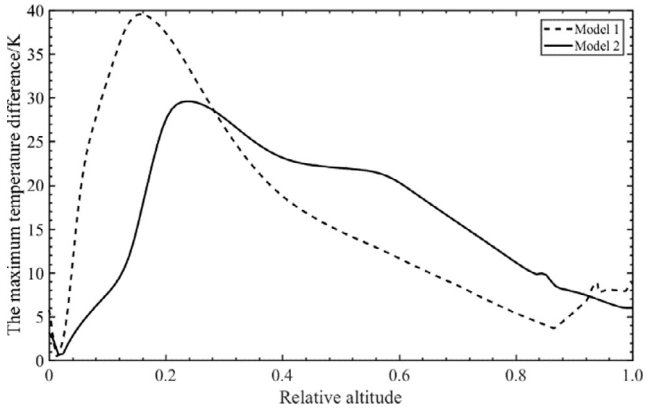

Fig. 13. The maximum temperature difference among three curves, uniform velocity, model 1 and 2.

Table 5
Simulation results of main parameters of IHX, Non-uniform velocity.

	Model	Simulation results	Targeted values	Error (%)
Heat Transfer (MW)	1	364.0	350	4.01
	2	362.1		3.47
Outlet Temperature of shell-side sodium (K)	1	626.9	625	0.3
	2	627.1		0.33
Outlet Temperature of tube-side sodium (K)	1	783.0	770	1.69
	2	774.9		0.64

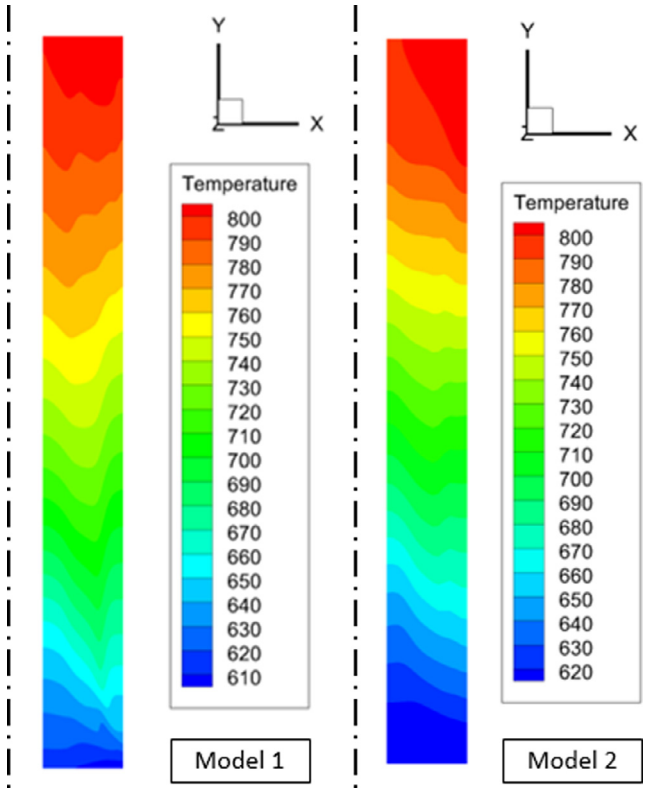

Fig. 14. Temperature distribution of shell-side sodium of model 1 and 2, non-uniform velocity.

velocity conditions. As shown on Fig. 18 shows that the two curves have a lot of ups and downs. After tube-side sodium flow into the IHX, there is a considerable fall from 7 K to under 2 K. Then, the maximum temperature difference rockets by roughly 20 K from the bottom to a peak of just above 20 K in model 1, which exceeds the permissible upper limit of 20 K, and by 16 K to a peak of about 18 K in model 2, due to the temperature of inner measuring line lower than that of the other two lines. Although the situation begins to improve and the curves have a small drop from the highest point to 16 K approximately, temperature difference in model 1 rises again, reaching the second peak of 18 K at the relative altitude of about 0.5 and following a substantial decrease to 11 K between the relative axial position of 0.5 and 0.8. The curve reaches the third peak of 18 K at the relative altitude of 0.92 because of a moderate fall in the temperature of outer measuring line. The curve of model 2 declines dramatically between the relative axial position of 0.4 and 0.75 to just above 5 K, following a slight fluctuation until the tube-side sodium flowing out of the Intermediate Heat Exchanger.

The distribution of the radial velocity of shell-side sodium on the x – y plane is depicted in Fig. 19. It can be seen that the radial velocity is almost 0 except in the vicinity of the inlet and outlet of both models. When the fluid flows into the middle region of the IHX, due to a large flow resistance on the radial direction, shell-side sodium mainly flows axially and downward. Therefore, the flow-induced vibration caused by large radial velocity more likely occurs near the region that sodium flows in and out of the IHX. Model 2 enlarges the inlet and out area for the shell-side sodium, reducing the average flow rate at the same time. Only in the small part near the outlet of model 2, the radial velocity exceeds the design upper limit of 0.73 m/s. Table 6 shows the pressure drops in both sides. When the inlet and outlet flow areas are enlarged, the pressure drop after the shell-side sodium pass though the IHX declines, which is a favorable factor.

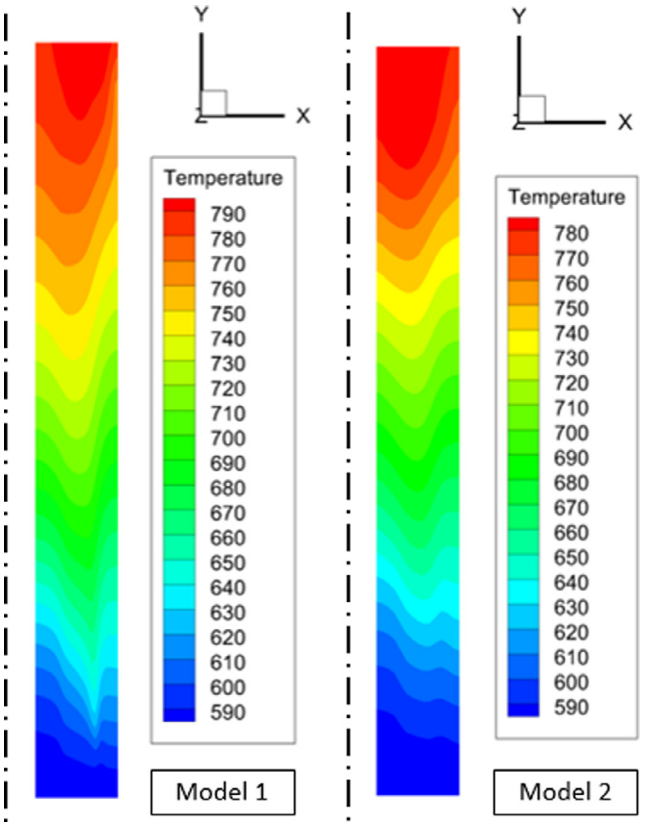

Fig. 15. Temperature distribution of tube-side sodium of model 1 and 2, non-uniform velocity.

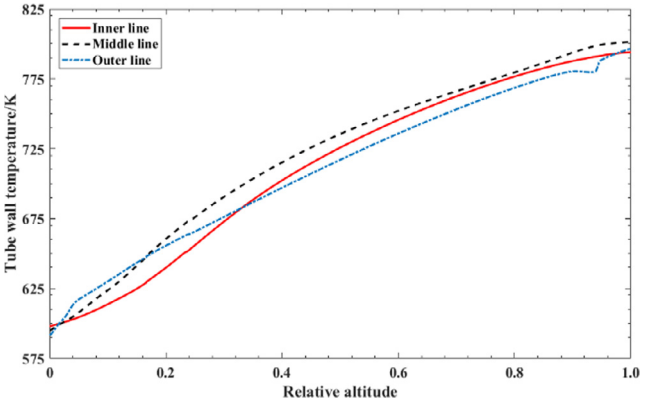

Fig. 16. The wall temperature vs. axial position, non-uniform velocity, model 1.

5. Conclusions

In this work, computational fluid dynamics codes, ANSYS FLUENT, is employed to simulate the temperature distribution and flow behaviors of liquid sodium in the Intermediate Heat Exchanger of the sodium-cooled fast reactor at full power conditions, with the porous media approach. The result of main parameters, such as

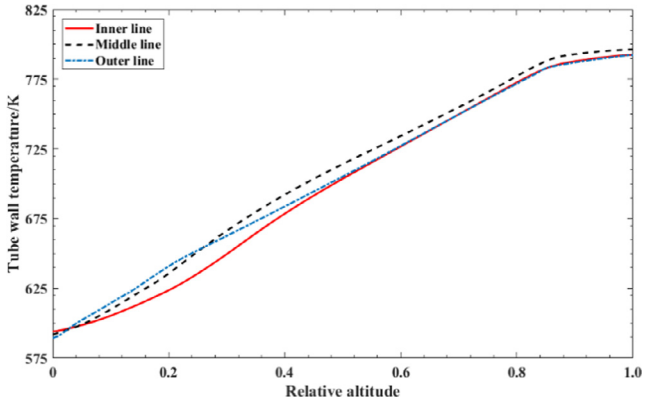

Fig. 17. The wall temperature vs. axial position, non-uniform velocity, model 2.

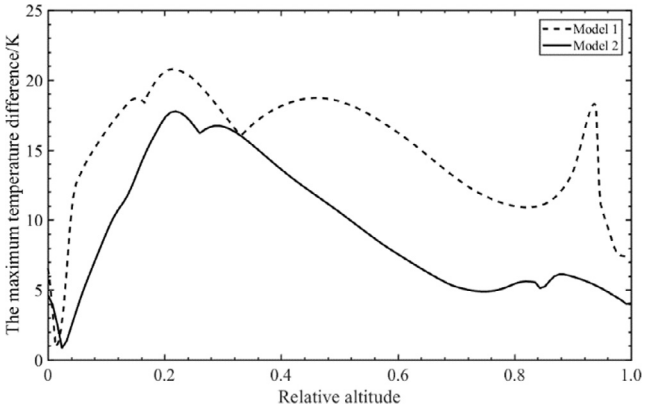

Fig. 18. The maximum temperature difference among three curves, non-uniform velocity, model 1 and 2.

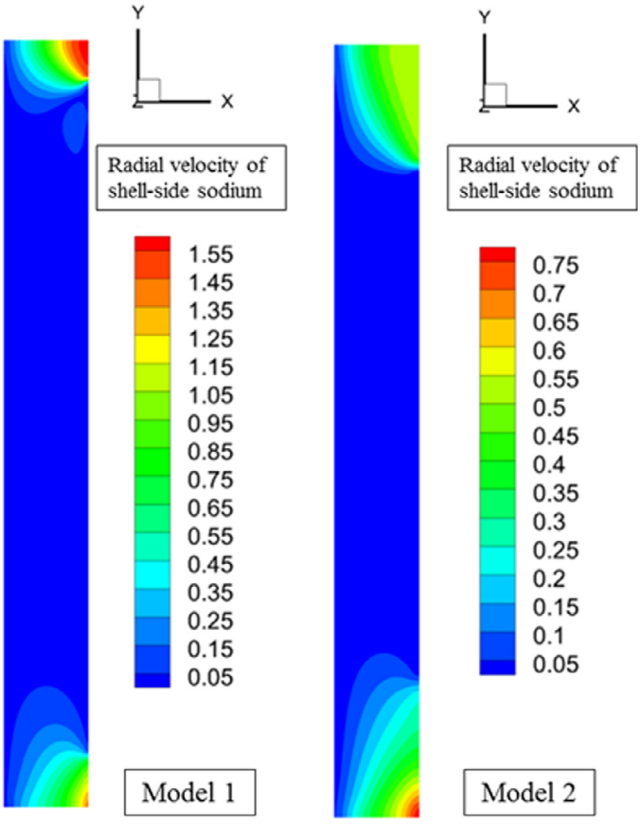

Fig. 19. The radial velocity contour of shell-side sodium in model 1 and 2, uniform velocity.

Table 6
The pressure drop (Pa).

Tube-side inlet	Model 1		Model 2	
	Uniform	Non-uniform	Uniform	Non-uniform
Shell-side	6622.41	6443.77	5448.85	5122.42
Tube-side	14900	15053	14900	15035

heat transfer values, the outlet temperature of the sodium on shell and tube side, agrees with assumed requirements and the fractional error is less than 5%.

- First for a theoretical case of uniform secondary sodium inlet flow distribution. Two models show that the heat exchange tubes at outer rows have the highest temperature, and temperature of the middle rows is greater than the inner rows. The maximum temperature differences among the three measuring lines are 40 K in model 1 and 30 K in model 2, which both have exceeded the permissible upper limit of 20 K.
- When tube-side sodium has a non-uniform entry, heat exchange is strengthened for outer rows of tubes. The temperature curves of three measuring lines are closer to each other. The maximum difference of model 1 is about 25 K, and model 2 is less than 20 K, which meets the design requirements of 20 K. Therefore, the use of an appropriate flow distribution device that can divert more flow towards outer rows to enhance the heat transfer in the outer rows, which could reduce the temperature gradient further and avoid reducing the stability of the welding equipment.
- The radial velocity of shell-side sodium tends to be higher when fluid just enters and before flow out of the IHX. In order to alleviate flow-induced vibration caused by a large radial velocity of the shell-side fluid, it should be appropriate to enlarge the inlet and outlet area.
- The results of the temperature distribution inside the IHX provide the basic data for the next step of thermal stress analysis. In addition, the calculation of the fluid flow field provides a reference for the future structural design of the IHX to avoid flow-induced vibration and other issues.
- All the simulations in this work are proofed to be meshed independent, by comparing the results from standard mesh and finer mesh (with approximately 3,000,000 cells), which shows no significant differences.

References

ANSYS Inc., Fluent theory Guide; 2013.
Boyd, C.F., Hardesty, K. CFD Analysis of 1/7th Scale Steam Generator Inlet Plenum Mixing During a PWR Severe Accident. USA: U.S. Nuclear Regulatory Commission; 2003, NUREG-1781.
Dehbi, A., Badreddine, H., 2013. Cfd prediction of mixing in a steam generator mock-up: comparison between full geometry and porous medium approaches. Ann. Nucl. Energy 58 (58), 178–187.
Gajapathy, R., Velusamy, K., Selvaraj, P., Chellapandi, P., Chetal, S.C., Sundararajan, T., 2008. Thermal hydraulic investigations of intermediate heat exchanger in a pool-type fast breeder reactor. Nucl. Eng. Des. 238 (7), 1577–1591.
Genić, S., Arandjelović, I., Kolendić, P., Jarić, M., Budimir, N., Genić, V., 2011. A review of explicit approximations of colebrook's equation. FME Trans. 39 (2), 67–71.
Haibo, L., Baoshan, J., Yu, Y., 2006. Application of porous medium method in study of TACR Calandria. Nucl. Power Eng. 27 (3), 24–27.
Idelchik, I.E., 1966. Handbook of hydraulic resistance, coefficient of local resistance and of friction,AECTR-6630.
Kaviany, M., 1995. Principles of Heat Transfer in Porous Media. Springer-Verlag.
Khair, K., Baset, S., Dimitrov, L., Millard, J. 2008. Numerical simulation of fluid flow and heat transfer in the advanced CANDU® reactor endshield using ANSYS-CFX and porous media approach. In: International Conference on Nuclear Engineering, 246–250.
Liu, Q., Ma, L., Xiang, S., 2013. Data Manual of Chemical and Physical Properties (inorganic, vol.) (fine). Chemical Industry Press.
Pilehvar, A.F., Aghaie, M., Esteki, M.H., Zolfaghari, A., Minuchehr, A., Daryabak, A., et al., 2013. Evaluation of compressible flow in spherical fueled reactors using the porous media model. Ann. Nucl. Energy 57 (5), 185–194.
Suyambazhahan, S., Das, S.K., Velusamy, K., Sundararajan, T., 2014. A computational study of flow mal-distribution on the thermal hydraulic performance of an intermediate heat exchanger in LMFBR. J. Nucl. Sci. Technol. 51 (6), 845–857.
Tochio, D., Fujimoto, N., 2016. Thermal mixing characteristics of helium gas in high-temperature gas-cooled reactor, (i) thermal mixing behavior of helium gas in HTTR. J. Nucl. Sci. Technol. 53 (3), 1–7.
Wang, X., Chang, H., Corradini, M., Cong, T., Wang, J., 2016. Prediction of falling film evaporation on the ap1000 passive containment cooling system using ANSYS fluent code. Ann. Nucl. Energy 95, 168–175.
Zarifi, E., Jahanfarnia, G., Veysi, F., 2013. Thermal–hydraulic modeling of nanofluids as the coolant in vver-1000 reactor core by the porous media approach. Ann. Nucl. Energy 51, 203–212.